

Motor State Prediction and Friction Compensation based on Data-driven Techniques

Nimantha Dasanayake^{1*} and Shehara Perera²

^{1*}Department of Mechanical Engineering, University of Moratuwa,
Katubedda, Moratuwa, 10400, Western Province, Sri Lanka.

²Department of Engineering, University of Cambridge, The Old Schools,
Trinity Lane, Cambridge, CB2 1TN, England, United Kingdom.

*Corresponding author(s). E-mail(s): dasanayakenp.21@uom.lk;
Contributing authors: ulsp2@cam.ac.uk;

Abstract

In order to provide robust, reliable, and accurate position and velocity control of motor drives, friction compensation has emerged as a key difficulty. Non-characterised friction could give rise to large position errors and vibrations which could be intensified by stick-slip motion and limit cycles. This paper presents an application of two data-driven nonlinear model identification techniques to discover the governing equations of motor dynamics that also characterise friction. Namely, the extraction of low-power data from time-delayed coordinates of motor velocity and sparse regression on nonlinear terms was applied to data acquired from a Brushless DC (BLDC) motor, to identify the underlying dynamics. The latter can be considered an extension of the conventional linear motor model commonly used in many model-based controllers. The identified nonlinear model was then contrasted with a nonlinear model that included the LuGre friction model and a linear model without friction. A nonlinear grey box model estimation method was used to calculate the optimum friction parameters for the LuGre model. The resulting nonlinear motor model with friction characteristics was then validated using a feedback friction compensation algorithm. The novel model showed more than **90%** accuracy in predicting the motor states in all considered input excitation signals. In addition, the model-based friction compensation scheme showed a relative increase in performance when compared with a system without friction compensation.

Keywords: Nonlinear dynamics, system identification, sparse regression, friction characterisation, motor control

1 Introduction

Friction identification and compensation play a major role in actuator control of mechatronic systems. This ensures that large positional errors, stick-slip effects and limit cycles are avoided to achieve smooth and accurate trajectories [1, 2]. The highly nonlinear nature of rotor dynamics mainly due to friction, makes it a difficult task to identify a proper mathematical model to build high-performance controllers.

Friction modelling dates back to the 90s, when researchers started looking for novel models to accurately model frictional forces, thus achieving better control of systems with friction ([3]). Typical friction components that are manifested in experimental data can be identified as, Coloumb, Stribeck and Viscous. With the advancement of research on friction modelling and parameterization, it was found that the friction regime was basically comprised of pre-sliding friction and sliding friction. Some literature also includes an intermediate regime called transition friction. [2, 4, 5].

Researchers in many different subfields of control engineering have been interested in friction compensation. For instance, robotics, autonomous systems and vehicle dynamics are a few of many that could benefit hugely by applying friction compensation and achieving reliable and robust control over their inherently nonlinear systems.

The major contribution of this research is twofold. Firstly, existing knowledge of data-driven nonlinear system identification techniques is leveraged to build a relatively accurate motor model which accounts for the nonlinear friction. Secondly, the identified model was integrated with a disturbance torque observer to extract and compensate for the external reaction forces applied on the motor rotor. More specifically, a feedback friction and reaction torque compensation algorithm was developed to ensure the position and velocity tracking with lower error.

This article is organized as follows. In section 2, motor and friction models used by state-of-the-art controllers will be discussed with an emphasis on the specific model used to validate the performance of the new method proposed in this work. In section 3, friction compensation techniques will be discussed and in section 4, the nonlinear system identification techniques will be comprehensively discussed. Then in section 5, the system identification and friction compensation techniques used in this work will be discussed. In section 6, the results of the overall system will be presented. The article will be concluded in section 7 with a description of the future directives.

2 Motor and Friction Models

The governing equations of the standard linear motor model can be expressed as follows:

$$J\dot{\omega}_m = K_t I - F - T_L \quad (1)$$

$$L\dot{I} = -RI - K_b\omega_m + V_{cmd} \quad (2)$$

Here, $J = J_m + J_w/G^2$ is the combined inertia of the rotor (J_m) and the load (J_l) and G is the gear ratio between the motor and the drive shaft. Furthermore, ω_m is the motor speed, I is the motor current, F is the frictional torque, T_L is the motor

load torque, V_{cmd} is the commanded voltage and, R and L are the resistance and the inductance of the rotor winding. Then, K_t , K_b represents the torque and back-EMF constants. The model described by the Equations (1) and (2) may incorporate nonlinearities in the friction term (F). Various models have been introduced in the past to capture these nonlinearities as accurately as possible.

2.1 Friction Models

According to the results of the studies, the frictional forces between two contacting surfaces are caused by asperities at the microscopical level. The effects of these asperities are dependent on factors like displacement and relative velocity of the surfaces, presence of lubrication, normal forces and temperature [1]. This gives rise to more than one regime of frictional behaviour: pre-sliding, transition and gross sliding [6].

Different models, that capture the friction components in different levels have been proposed previously [7]. These models can be basically categorized as static and dynamic models. In static models, friction only depends on the velocity while in dynamic models, friction also depends on the deformation of the asperities. Static friction models consist of the friction components, Coloumb, Stribeck and Viscous. There is a discontinuous jump in friction at pre-sliding due to Coloumb friction and it has been replaced by a continuous line of finite slope to ensure the continuity that is needed for control systems [4]. Karnopp model was later developed [7] by adding a small region of zero velocity to get rid of the difficulty in identifying very small velocities due to the finite resolution of angular measurement sensors. The weakness of the static models is the inability to capture the forces in a pre-sliding friction regime. Further studies have revealed that hysteretic displacement-dependent friction force is present in the pre-sliding region [6]. In addition, the hysteresis also incorporates a non-local memory characteristic. Several factors may decide the shape of the hysteretic function such as the distribution of the asperity heights, the tangential stiffness, and the normal stiffness of the contact [6]. In addition to hysteresis, there are three other properties (see figure 1), namely frictional lag, periodic friction and non-drifting properties which are considered to be essential to be modelled by a successful friction model. A comparison of these characteristics for different friction models has been presented in [8].

In generic friction model, the friction force is represented as a function of the position, velocity and an internal state (z) which is considered as the deflection of the asperities in the contact surfaces. And it is incorporated with a first order differential equation that describes the dynamics of the internal state.

$$F_f = f(x, v, z) \quad (3)$$

$$\frac{dz}{dt} = g(x, v, z) \quad (4)$$

To create an accurate friction model, the proper functions for f and g are thus found empirically. In doing so, two conditions of motion is considered. First one is the steady state when internal state is non varying. In this situation,

$$g(x, v, z) = 0 \quad (5)$$

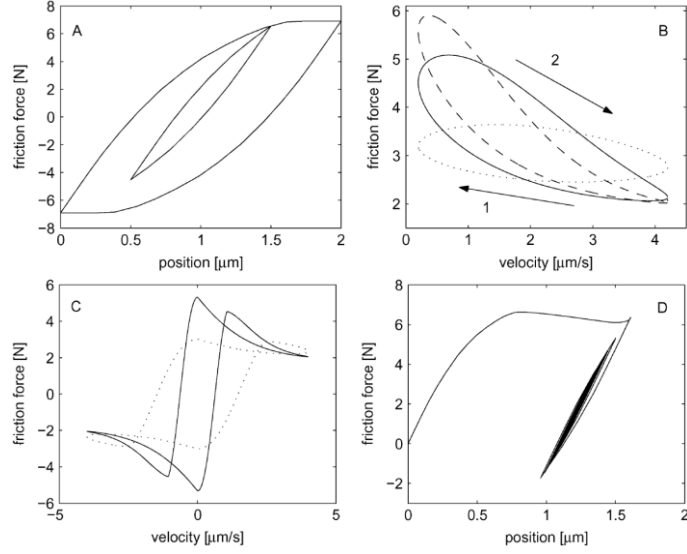


Fig. 1: The four main properties of friction A - hysteresis, B - frictional lag, C - periodic friction and D - non-drifting property [9]

$$f(x, v, z) = s(v) + f_2(v) \quad (6)$$

where $s(v)$, is the Stribeck curve. It is a decreasing function for increasing velocity bounded by an upper limit equal to the static friction and a lower limit equal to the Coulomb friction. So it can be seen that friction is purely a function of the velocity. $s(v)$ is the Stribeck function, which decreases when velocity increases until a characteristic velocity called Stribeck velocity is achieved. $f_2(v)$ is the viscous function that gives the viscous friction component. The most common form of Stribeck curve is given by the following Equation,

$$s(v) = F_c + (F_s - F_c)e^{-\left|\frac{v}{v_s}\right|^\delta} \quad (7)$$

where F_c is the Coloumb friction force and F_s is the stiction force which is the force additional to F_c that acts on the system just before sliding happens. v_s is called the Stribeck velocity, beyond which, the friction starts to increase.

The second condition considered in empirical evaluation of the friction models is pre-sliding condition when displacements are very small. In this condition, the friction force exhibits the hysteretic behaviour with non-local memory characteristics against displacement. There are two main types of hysteretic behavior. First type is the hysteresis with non-local memory: which means that the future values of the friction force at some instant of time $t(t > t_0)$ depend not only on its present value at the instant of time t_0 and the value of the displacement in but also on the past maximum values of the friction force. This property is in contrast to the behavior of hysteresis nonlinearities with local memory: the second type, where the past has its influence upon the future through the current value of the friction [10]. The friction force is expressed as a hysteresis function in Equation 8.

$$F_f = f(x, v, z) = F_h \quad (8)$$

Here F_h is the hysteresis function. A generalized parametric form of equation (6) can be expressed as,

$$\frac{dz}{dt} = v \left(1 - \frac{z}{g(t)} \right) h(t) \quad (9)$$

where $g(t)$ and $h(t)$ are functions to be determined.

The first dynamic friction model that was developed is called the Dahl model. This model not only captures the pre-sliding behaviour but also the hysteresis effect. The friction force is a hysteresis function of the displacement without memory [6]. The position dependence but velocity independence of pre-sliding friction (rate independence) was characterised firstly by the Dahl model. If the external force is not enough to exceed static friction, the asperities at the contact surface will deform resulting in a pre-sliding motion [11]. The force in Dahl model is characterized by the following function.

$$F_f = kz \quad (10)$$

$$\frac{dz}{dt} = v \left(1 - \operatorname{sgn}(v) \frac{\sigma_z}{F_c} \right) \quad (11)$$

Comparing with the general form in Equation 8, here $h(t) = 1$ and $g(t) = \frac{F_c}{k}$. Here, k is the stiffness of the asperities. However, as it can be seen from Equations 10 and 11 Dahl model does not capture stiction or Stribeck friction which are rate dependent. As a result many enhanced models that capture those effects has been developed later on. In the popular LuGre model, the asperities are modeled as small bristles (known as the bristle model). Compared to Dahl model, this model captures the Stribeck and viscous effects. The equations are as follows [5].

$$F_f = kz + \sigma \frac{dz}{dt} + \alpha_2 v \quad (12)$$

$$\frac{dz}{dt} = v \left(1 - \operatorname{sgn}(v) \frac{kz}{s(v)} \right) \quad (13)$$

$$s(v) = \alpha_0 + \alpha_1 e^{-\left(\frac{v}{v_s}\right)^2} \quad (14)$$

When compared with the general parametric model represented by Equation 8, $g(t)$ has been converted to an implicit function of time that depends of velocity, i.e $\frac{s(v)}{k}$, and $h(t) = 1$. Equation 14 can be compared with Equation 7 and it can be seen that δ has been chosen as 2 and the stiction and Coulomb friction have been replaced by two parameters $\alpha_0 = F_c$ and $\alpha_1 = F_s - F_c$. Here, α_2 is the viscous friction coefficient. It is evident that LuGre model has been used in many applications in developing control systems with friction compensation [12–14].

One drawback of the LuGre model can be identified as the non-differentiable point at breakaway velocity. To overcome this issue a new continuously differentiable friction

model has been proposed in [15] and applied in [2]. Furthermore, the LuGre model lacks the non-drifting property (shown in Figure 1 - D) which was later extended using an elastoplastic model of bristles instead of the pure elastic model [9]. However, the hysteresis behaviour of friction has been found to be with a non-local memory (see [9]) which is not characterised by Dahl or LuGre models. Attempts have been made to modify the model so that this property is captured. For instance Leuven model [16, 17] introduces a hysteresis function (F_h) to the LuGre model as follows,

$$F_f = F_h(z) + \sigma \frac{dz}{dt} + \alpha_z v \quad (15)$$

$$\frac{dz}{dt} = v \left(1 - \text{sgn}(v) \frac{F_h(z)}{g(v)} \right) \quad (16)$$

However, due to too much complication of the model, it is difficult to implement it. In addition, in both LuGre and Leuven models, it is assumed that the general function $h(t) = 1$, but the experiments reveal otherwise [8]. This was the main motivation to develop a model that replaces the hysteresis function with a Maxwell Slip model representation called the Generalized Maxwell Slip (GMS) model. Maxwell slip model considers the asperities as elastoplastic elements and models them as spring mass systems having a spring stiffness (k) with a force limit (W). Then it is considered that all the elements are connected in parallel, so the external force affects all the elements at once. The main target of this distributed element model is to capture the hysteresis with non-local memory and is extensively elaborated in [18]. If the i^{th} element sticks, the elementary friction force F_i is proportional to the deflection of the corresponding asperity, which can be modelled as:

$$F_i = k_i z_i \quad (17)$$

$$\frac{dz_i}{dt} = v \quad (18)$$

In GMS model, the function $h(t)$ is evaluated using experimental data obtained for a chosen unidirectional velocity function [8]. Frictional memory in sliding regime is the dominant feature that enables this evaluation. According to [8], the evaluated function is of the following form,

$$h(t) = \frac{C}{|v|} \quad (19)$$

Here C is an attraction parameter which determines how fast the internal state reaches its limit. The sliding regime equation is thus obtained for the GMS by substituting Equation 19 to Equation 9 and replacing $g(t)$ with $s(v)$ as in Equation 13.

$$\frac{dz}{dt} = \text{sgn}(v) C \left(1 - \frac{kz}{s(v)} \right) \quad (20)$$

Now, to obtain the hysteresis effect with non-local memory in the pre-sliding regime, 20 is applied to each element of the GMS model. This results in,

$$\frac{dz_i}{dt} = \text{sgn}(v) C_i \left(1 - \frac{k_i z_i}{s_i(v)} \right) \quad (21)$$

where, the index i denotes the i^{th} element. The friction force is given by,

$$F_f = \sum_{j=1}^N \left(k_j z_j + \sigma_j \frac{dz_j}{dt} \right) + \alpha_2 v \quad (22)$$

where N is the number of elements. The first term of the Equation 22 under summation is called the elasto-sliding force. Thus the GMS model in both sticking and slipping conditions can be expressed as,

If sticks:

$$\frac{dz_i}{dt} = v \quad (23)$$

the element keep sticking until $z_i > s_i(v)$

If slips:

$$\frac{dz_i}{dt} = \text{sgn}(v) C_i \left(1 - \frac{z_i}{s_i(v)} \right) \quad (24)$$

Thus the element keeps slipping until velocity goes through zero. A problem immediately arises due to this formulation since the number of parameters to estimate is high. This number can be reduced without sacrificing the essence of this model, by assuming one common form of the Stribeck curve and attraction parameter for all elements, i.e. $s_i(v) = \mu_i S(v)$ and $C_i = \mu_i C$, where μ_i is a scaling parameter. After doing so, the Equation 24 becomes,

$$\frac{dz_i}{dt} = \text{sgn}(v) C \left(\mu_i - \frac{z_i}{S(v)} \right) \quad (25)$$

Several work has been carried out out to compare the friction models discussed so far. In [5] GMS models with 4 and 10 elements have been compared with the LuGre model and it has been shown that GMS models outperform LuGre. In [9] GMS model of up to 10 blocks has been tested and concluded that at least 4 blocks are essential to accurately model the friction. In [19] shows that the GMS model performs better than LuGre. This proves that GMS captures most of the friction properties and gives better predictions when compared with other models. But for the downside, it must also be mentioned that to identify the parameters, high-resolution position measurement is needed.

In addition to the friction models discussed so far, other friction models like, the continuously differentiable friction model based on hyperbolic tangent functions [15, 20], a model based on Fourier series [21], and 3rd order polynomial based friction model [22] which includes extended terms for Coulomb and viscous friction could be found in literature.

3 Friction Compensation

In order to compensate for friction in motor drives, many methodologies have been put forth that take into account various types of friction phenomena, various models

to represent them, and various strategies to remove or satisfactorily decrease their negative impacts on the motion. Starting from basic Coulomb and viscous friction compensation (see [20]), this subject extends to a wide range of control algorithms. In this section, we will have brief visits on four categories of friction compensation namely, feedforward and feedback compensation, compensation in variable structure systems, observer-based compensation and adaptive friction model-based compensation.

3.1 Feedforward and Feedback Compensation

The common feature seen in feedforward compensation is that it uses the reference inputs (typically position or velocity) to predict the future force values [4, 5, 19]. A compensation scheme based on estimating the inertia and friction forces by feedforward reference position and then modifying the control signal coming from a Proportional Derivative (PD) control has been proposed in [4]. A similar approach but with the LuGre model has been implemented in [5] and has achieved more than 80% reduction in positional error relative to the control without compensation. In [23], the feedforward term also incorporates a term that accounts for the velocity error. In addition, a cost function with weighted squared state error and control effort has been used and the optimal value for the control gain is calculated using the LQR technique. In contrast to feedforward compensation, the feedback compensation technique uses the measured outputs i.e. position and velocity to estimate the friction force. Then is it fed back to the control signal with a gain. Most of the systems developed so far use the LuGre model for this estimation [24, 25]. A comparison between the two approaches can be done using the block diagrams shown in figure 2.

3.2 Compensation in Variable Structure Systems

Variable Structure Systems (VSS) are the systems that vary the control model structure to compensate for the nonlinearities. VSS are suitable for control of the systems that are modelled with nonlinear friction forces. For instance, sliding mode control (SMC) has been applied in the literature to achieve robust position and/or velocity tracking [2, 12, 13, 26]. In [2], an adaptive robust controller has been designed with a continuous friction model, while an adaptive funnel sliding mode control is used in [26]. A funnel sliding mode control has an adaptive gain ($u = \tau e$, u is the control, e is the error and τ is the adaptive gain) that increases as the error reaches a

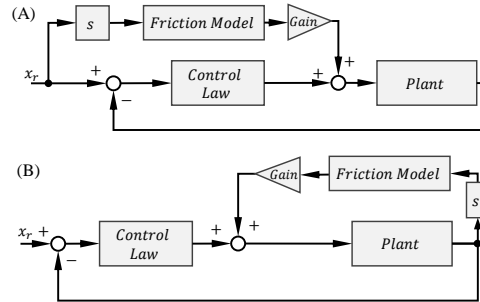


Fig. 2: Comparison of two common friction compensation algorithms, (A) Feedforward, (B) Feedback

funnel shape function ($F(t)$) around time axis of error vs time graph. In addition, a modified Stribeck friction with \tanh function has been used for the LuGre model to eliminate the discontinuity, so that it can be used for backstepping [26]. An interesting approach can be found in [27], where the friction is not compensated in occasions where it acts as a restoring force to bring back the dynamics onto the sliding surface. Another example of a VSS is the robust integral of the sign of the error (RISE) feedback term is employed to design an innovative adaptive controller to compensate for nonlinear friction and bounded disturbances [20].

3.3 Observer based Compensation

Observers have been used to estimate the internal variable (asperity deformation), thus estimating the friction [7, 28]. A non-model-based extended state reduced order observer (ESO) with only first order derivatives has been developed for robot joint motion in [29]. Another ESO-based control approach can be found in [30].

Furthermore, the Extended Kalman-Bucy filter (EKF) has been used together with a dynamic friction model to observe the friction force under varying normal load conditions [28]. The system is adaptive to normal load changes and they have tried both LuGre and Dahl models. Around 75% decrease in error when compared with PID control without friction compensation can be seen in the results. In addition, observers based on LuGre, Dahl and Bliman-serine models are discussed in [7].

3.4 Adaptive Friction Model based Compensation

Although friction has been modelled accurately enough to improve the position and velocity tracking of systems, it is noteworthy that unless these models are adaptive, they can give inaccurate friction estimates due to uncertainty of model parameters. This uncertainty is mainly caused by changes in operating conditions like temperature, lubrication and normal load. Many adaptive friction compensation methods have been thus developed. For instance, the adaptive compensation strategy discussed in [5] has considered the Coulomb friction and Viscous friction as the adaptive parameters of the LuGre model since these have the most significant effect on the accuracy of friction estimation. The two parameters have been multiplied by two gains, which are updated according to a law that accounts for the error in the tracked position. In [12] a similar formulation, an adaptive LuGre model has been used to compensate friction in an adaptive SMC scheme known as adaptive non-singular fast terminal SMC. Furthermore, an adaptive robust control implemented for position tracking using a novel continuous friction model can be seen in [2].

Previous work could be found where emphasis was given to studying friction variation with temperature. One approach is to develop an exponential function-based model using the experimental data to represent the temperature effects on friction. Here, a 3rd order polynomial form of friction model that includes extended terms for Coulomb and viscous components has been used and the LuGre and GMS models has been modified with load and temperature dependant terms [22].

Parameter identification and calibration of adaptive compensation schemes is an important aspect to make sure the model matches the current operating condition.

This has been achieved using Bayesian inference in [14] for a LuGre model. Here, separate calibrations are done for presiding and gross sliding regimes based on comparative features, the external force applied and pre-sliding displacement respectively. The parameter identification can also be done using velocity, friction data and regression [19]. Another method used for an improved LuGre model, is adding normal load-dependent terms to Coulomb friction thus the system automatically adapts to varying load conditions. Furthermore, optimization methods like differential evolution algorithm, genetic algorithm (GA) and particle swarm optimization (PSO) have been utilized for online identification of static and dynamic parameters [24, 25]. In the work presented in [24] the parameter identification for the LuGre model has been done using high-precision measurement of friction torque, based on a disturbance observer (DOB). A high-precision torque sensor has been used to calibrate the observer.

3.5 Nonlinear Control based Compensation

The Discontinuous Nonlinear Proportional Feedback (DNPF) method has been proposed in [4] where a fixed compensation friction that is slightly larger than the Coulomb friction (calculated experimentally) is added to the control signal when the displacement becomes lower than the pre-sliding distance. In addition, a gain scheduling-based PD controller has been tested in this work. The scheme has two controllers one for pre-sliding other for gross sliding regime which has the gain scheduling to have dynamic friction parameters. Testing has shown that both nonlinear control methods outperform the linear feedforward method in the sense of a fast response and low steady-state error.

3.6 ANN and other intelligent algorithms based Compensation

An adaptive SMC using neural network is designed to approximate the nonlinear friction can be found in [13]. Here, a neural network control is integrated into the SMC to enhance the robustness. In [26] an Artificial Neural Network (ANN) has been employed to approximate the friction and other nonlinearities. The LuGre friction model has been established on the basis of the measured experimental data and a two-step parameter identification process with a GA. In the first step of parameter identification, static parameters were identified using the Stribeck curve using the GA and in the second step, dynamic parameters were identified from the data from presliding regime and the GA [31].

4 System Identification

The extraction of governing equations from data is a major challenge in many scientific and engineering domains. [32]. This is particularly noticeable in nonlinear systems. For example, mechanical systems that experience friction are challenging to regulate in the absence of a precise model that incorporates nonlinear dynamics. The authors of this study have concentrated on two particular methods for determining the underlying nonlinear dynamics of systems with a plurality of physics that have

been recently improved and employed in a variety of contexts. The major contribution of this research is the application of these popular techniques on friction model identification in an electric motor. This section will begin with a brief overview of the so-called SYNDYc ([33]) techniques. Next, the theory behind time delay embedding (TDE) and Dynamic Mode Decomposition (DMD) will be described, along with some insights regarding Koopman theory ([34]), which the authors used to determine the dynamics of the internal variable of friction.

4.1 Sparse Identification of Nonlinear Dynamics with Control (SINDYc)

SINDY is an algorithm designed to extract parsimonious dynamics from time-series data using a regression method. Models for fluid flows, optical systems, chemical reactions, plasma convection, structures, and model predictive control have all been identified through the extensive use of SINDY. [35]. For most of the physical systems, it can be assumed that the structure of the governing equation only contains few important terms so that the equations are sparse in the space of possible functions [32]. Under this assumption, sparsity promoting techniques in corporation with machine learning have been used to discover nonlinear dynamics through regression of data. For examples, [32] presents the results of predicting the dynamics of a simulated chaotic Lorenz system and vortex shedding of a flow passing a cylinder with high accuracy. The SINDY algorithm has been generalized to systems with external control inputs[33]. An advantage of this method is balancing model complexity with descriptive ability, and thus promoting interpretability and generalizability [35]. Further advancement of SYNDY could be observed in in [35] where it has been integrated with an auto encoding ANN. The autoencoder is used to find appropriate coordinates for SYNDY model by dimensional reduction. It has shown promising results on some example dynamical systems like Lorenz system, reaction diffusion and nonlinear pendulum.

4.2 Time Delay Embedding and Dynamic Mode Decomposition

Much work has gone into determining the proper coordinate transformations to apply to measurement data of a dynamical system in order to approximate the nonlinear dynamics using a higher order linear system [35–37]. The Koopman Theory is the primary motivator behind the idea of utilizing a linear system to approximate nonlinear dynamics [34]. In essence, the theory states that a finite dimensional nonlinear dynamical system can be represented by an infinite-dimensional system that is constructed by observable functions of the states lying in a Hilbert space. An infinite dimensional linear operator acting on the observable functions describes the flow of these observables along the trajectories of the system. Koopman theory has been used commonly in fluid dynamics [38] and discovering dynamics of chaotic systems [37].

Recent developments in the field of data-driven model identification, various techniques have been tested to find an approximated finite dimensional subspace of the Koopman observables, so the theory can be practically implemented to predict the behaviour of nonlinear dynamical systems. For high dimensional systems this has been done using a method called Hankel Alternate View of Koopman (HAVOK) that is

based on time delay embedding and DMD [37]. HAVOK has been applied to predict the dynamics of chaotic systems like Lorenz attractor. It has also been applied to identify the unknown dynamics of soft robots [39].

When the full state of the dynamical model is not measurable due to the existence of hidden variables, or lack of measured data, it is possible to reconstruct the underlying dynamics of the system approximately using a higher dimensional model that has time-delayed versions of the available state measurements as new states [36]. By singular value decomposition (SVD) of the delay coordinates and DMD of the Eigenmode time series data, a promising low dimensional approximation to a Koopman system could be obtained [37]. DMD can also be done to forced nonlinear systems and the method is comprehensively discussed in [40]. As a further development, in [41] autoencoders have been incorporated with Time Delay Embedding and SYNDy algorithm with appropriate loss function to reconstruct the hidden dynamics of the system with only one known state.

The authors were motivated by the fact that it is possible to reconstruct the unavailable or hidden system states if only data of one or few states are available. This led to the hypothesis: the hidden variable of friction (asperity deformation, as described in the Section 2) can be reconstructed using velocity data by choosing a proper order for time delay embedding and extracting components relevant to low power singular values of SVD. Further details of the followed methodology by authors is presented in the Section 5.

5 Methodology

It was ascertained through the study of state-of-the-art that fewer attempts have been put on incorporating the data-driven methods to build motor models that account for frictional forces. Therefore, the main objective of this research was to discover how effective the data-driven methods are in replacing the conventional friction models to give better predictions on motor states. Specifically, the methodology followed in this research can be described in two steps: first, TDE was used to build up a high-order coordinate system from velocity data to extract the hidden variable of friction. As the second step, a data-driven nonlinear model identification method: SINDYc was used to fit a motor model incorporating hidden variable data extracted from the previous step. All data for the experiments were obtained by exciting a BLDC motor using an excitation signal that is described in subsequent sub-sections. Furthermore, three more excitation signals were devised to validate the models to see their ability to be generalized for a wider span of operating conditions. The data-driven method was then compared with the conventional linear motor model and a motor model with nonlinear friction. Considering all the friction models discussed in Section 2, it was decided to use the LuGre model considering its large number of practical implementations found in literature and the feasibility of determining the parameters correctly using a low-resolution position measurement.

5.1 Dynamic Models

For a rigorous treatment for the proof of the concept presented in this paper, it was necessary to compare three dynamic models: the first two models are existing ones and the third one is a novel model based on data-driven techniques, that was developed by authors.

The first model was the conventional linear motor dynamic model that considers only viscous friction which is described in the equation. The coefficients for the model was identified using linear regression. The method is not described here since it is insignificant to the focus of this paper.

The second model was obtained by modifying the first model by introducing the LuGre friction model. The parameter determination for this model will be described in detail in this section. The method was adopted from [5]. The static parameters of the LuGre model e.i. α_0 , α_1 , α_2 and v_0 were determined using low steady-state velocity responses of the motor to low excitation voltages, while the dynamic parameters e.i. σ_0 and σ_1 were identified using the estimation of a nonlinear grey box model. The initial values of the dynamic parameters for the estimation were calculated based on the current responses for slow ramp excitation voltages. The search method used is the Trust-Region Reflective Newton method of nonlinear least-squares. This is a constrained optimization method explained by the following equation,

$$\min_{\boldsymbol{\xi}} F(\boldsymbol{\xi}) = \min_{\mathbf{x}} \|\mathbf{y} - \mathbf{f}(\mathbf{x}, \mathbf{u}, \boldsymbol{\xi})\|_2^2 \quad (26)$$

where, $\mathbf{x} \in \mathbb{R}^n$ is the state vector, $\mathbf{y} = \dot{\mathbf{x}} \in \mathbb{R}^n$ is the derivative vector, $\mathbf{u} \in \mathbb{R}^m$ is the input vector, $\boldsymbol{\xi} \in \mathbb{R}^l$ is the vector of unknown coefficients and $\mathbf{f} : \mathbb{R}^n \rightarrow \mathbb{R}^n$ is a continuous function that defines the time evolution of the dynamical system by the following equation.

$$\frac{dx}{dt} = f(x, u) \quad (27)$$

In the Trust Region optimization method, the nonlinear function $F(\boldsymbol{\xi})$ is approximated by Taylor series for the 2^{nd} order and constrained on the so-called "trust region" where the approximation holds well enough. The constraint on the system is in the form of $\|\boldsymbol{\xi} - \mathbf{c}\|_2 < \delta$, where \mathbf{c} is the point around which the approximation is done. Then, the optimization problem in the Trust Region Reflective Newton method can be expressed as,

$$\min_{\boldsymbol{\xi}} F(\boldsymbol{\xi}) = \min_{\boldsymbol{\xi}} (f(\mathbf{c}) + \nabla f^T(\boldsymbol{\xi} - \mathbf{c}) + \frac{1}{2}(\boldsymbol{\xi} - \mathbf{c})^T H(\boldsymbol{\xi} - \mathbf{c})) \quad (28)$$

where, ∇ is the gradient operator and H is the Hessian matrix of $f(\boldsymbol{\xi})$. The solution for this problem is obtained by restricting the trust region sub-problem into a two-dimensional subspace as detailed in [42].

The third model was discovered using the SINDYc algorithm. It is noteworthy that this discovery becomes a major contribution to the research on motor friction modelling not only because of applying SINDYc on motor data but also using TDE to extract information about a hidden variable: the deformation of asperities (z). Therefore first, the formulation of the method of this extraction must be discussed.

The motivation towards using delay embedding was the inability to build a closed-form model analytically or using data-driven techniques when one or more variables of the dynamical system are hidden. In delay embedding, a latent high-dimensional system is built using incomplete measurements by expanding the measured state variables into a higher-order set of states made out of the time history of the measured states [36].

If $x(t)$ is the known, measured state in time t , its Hankel matrix, $\mathbf{H} \in \mathbb{R}^{n \times m}$ can be written as,

$$H = \begin{bmatrix} x(t_1) & x(t_2) & x(t_3) & \dots & x(t_n) \\ x(t_2) & x(t_3) & x(t_4) & \dots & x(t_{n+1}) \\ \cdot & \cdot & \cdot & & \cdot \\ \cdot & \cdot & \cdot & & \cdot \\ x(t_m) & x(t_{m+1}) & x(t_{m+2}) & \dots & x(t_{m+n-1}) \end{bmatrix} \quad (29)$$

where, m is the number of time delayed coordinates and n is the number of measured time instances. The Hankel matrix is then subjected to SVD, to obtain the time series composition of Eigen modes.

$$H = U \Sigma V^T \quad (30)$$

$$\Sigma = \begin{bmatrix} \sigma_1 & 0 & 0 & \dots & 0 \\ 0 & \sigma_2 & 0 & \dots & 0 \\ \cdot & \cdot & \cdot & & \cdot \\ \cdot & \cdot & \cdot & & \cdot \\ 0 & 0 & 0 & \dots & \sigma_m \end{bmatrix} \quad (31)$$

Here, $U \in \mathbb{R}^{m \times m}$ is the matrix with Eigen vectors arranged in columns. $\Sigma \in \mathbb{R}^{m \times m}$ is a diagonal matrix with eigenvalues arranged in descending order along the diagonal. $V \in \mathbb{R}^{m \times n}$ matrix that holds the information about how the composition of the eigenvectors in each time-delayed coordinate changes with time. The notion of the eigenvalues here is that it represents how strongly the corresponding eigencomponent influences the dynamics of the time-delayed coordinates. Given the possibility that information about the asperity deformation is hidden inside velocity data, the authors' hypothesis was that this information must be represented by the lowest energy eigenvalues. The basis behind this thought lies in two facts, first that the magnitude of asperity deformation is of a very small scale when compared with other states (displacement, velocity and current) and the second is that this variable is dynamic only in a short time range since the deformation gets saturated after reaching its maximum value according to the empirical findings of friction behaviour.

Therefore, a method was formulated to rebuild the time-delayed coordinates after omitting prominent eigen components by introducing a modified matrix $\hat{\Sigma}$ which has a selected range (for example $(m - l_0)^{th}$ to $(m - l_0 + l_1)^{th}$) of low energy eigenvalues, instead of Σ .

$$\hat{\Sigma} = \begin{bmatrix} 0 & \dots & 0 & 0 & \dots & 0 & 0 & \dots \\ \vdots & \ddots & \vdots & \vdots & \ddots & \vdots & \vdots & \ddots \\ 0 & \dots & \sigma_{m-l_0} & 0 & \dots & 0 & 0 & \dots \\ 0 & \dots & 0 & \sigma_{m-l_0+1} & \dots & 0 & 0 & \dots \\ \vdots & \ddots & \vdots & \vdots & \ddots & \vdots & \vdots & \ddots \\ 0 & \dots & 0 & 0 & \dots & \sigma_{m-l_0+l_1} & 0 & \dots \\ 0 & \dots & 0 & 0 & \dots & 0 & 0 & \dots \\ \vdots & \ddots & \vdots & \vdots & \ddots & \vdots & \vdots & \ddots \end{bmatrix} \quad (32)$$

Now, the delay coordinates corresponding to low energy eigen components can be obtained as,

$$\hat{H} = U \hat{\Sigma} V^T \quad (33)$$

where \hat{H} is the new Hankel matrix with low energy delay coordinates. The first coordinate of \hat{H} can be directly used as a representation of a hidden variable, or a scaled version of it.

Now, given the measured data and after discovering hidden variable data, SINDYc algorithm was used to fit a nonlinear sparse model as described in [33]. Consider the system described by Equation 27. The algorithm first develops a library of candidate functions $\Theta(\mathbf{x}, \mathbf{u})$ which may also include essentially, nonlinear terms that are more likely to describe the underline dynamics of the system. If the functions are written in terms of the data matrices of state and control variables i.e $\mathbf{X} = [\mathbf{x}(t_1), \mathbf{x}(t_2), \dots, \mathbf{x}(t_n)]$ and $\mathbf{U} = [\mathbf{u}(t_1), \mathbf{u}(t_2), \dots, \mathbf{u}(t_n)]$, the candidate function library can be written as,

$$\Theta^T(X, U) = \begin{bmatrix} f_1(\mathbf{X}, \mathbf{U}) \\ f_2(\mathbf{X}, \mathbf{U}) \\ f_3(\mathbf{X}, \mathbf{U}) \\ \vdots \\ \vdots \end{bmatrix} \quad (34)$$

And then the system can be represented by the following equation,

$$\dot{X} = \Xi \Theta^T(X, U) \quad (35)$$

where Ξ is the coefficient matrix. Usually, the coefficients are then determined using a sparse regression algorithm because most of the nonlinear systems do not have the same nonlinear term repeated in many state equations. A common sparse regression algorithm used in literature is LASSO [43] i.e,

$$\xi_k = \operatorname{argmin}_{\xi_k} \|\dot{X}_k - \xi_k \Theta^T(X, U)\|_2 + \|\alpha \xi_k\|_1 \quad (36)$$

where ξ_k is the k^{th} row of the coefficient matrix Ξ and \dot{X}_k is the k^{th} row of the \dot{X} matrix. However, the method followed in this work is based on that is described in [33], where the resulting elements of Ξ after regression are hard thresholded one by one until it doesn't show a significant improvement in the model fit percentage (Equation 45) for the validation dataset.

Table 1: Motor Specifications

| Specification | Value | Unit |
|-----------------|-------|------|
| Nominal Voltage | 24 | V |
| Nominal Current | 6.39 | A |
| Stall Current | 111 | A |
| Nominal Speed | 2720 | rpm |
| Max. Speed | 5000 | rpm |
| Nominal Torque | 457 | mNm |
| Stall Torque | 7910 | mNm |

5.2 Experimental Setup

A BLDC motor (maxon international ltd.) with the specs given in table 1 with an inbuilt hall sensor system with the capability of measuring the angular displacement with a resolution of 5.45° was used to build a setup to experiment the feasibility of using data-driven methods to identify nonlinear motor models. In addition, the setup was used to test the model-based friction compensation.

5.3 Excitation Signal

The excitation signals e.i. the commanded voltage were selected based on the required operating amplitude and frequency range of the motor for an exoskeleton application. One signal was derived for model fitting and another 3 for validation. The modelling fitting signal depicted in Figure 3 (A) has an amplitude range of $0 - 12V$, and a frequency range of $0.1 - 1$ Hz. The first validation signal depicted in Figure 3 (B) has a lower amplitude and a frequency range of $0.05 - 1$ Hz. Furthermore, its frequency variation is slower. Therefore the signal (B) represents data from a different operating region of the motor in the sense of amplitude and frequency. To test the fitted model's performance in low amplitude the signal shown in Figure 3 (C) was used, which has an amplitude range of $0 - 0.5$ V and a frequency range of $0.25 - 1$ Hz. Then the step signal with step amplitudes between $0 - 10$ V was used as shown in Figure 3 (D). The sampling time of all the signals was 12 ms.

5.4 Friction Compensation

The model identified using sparse regression was used to derive a function for friction force. Then a friction compensation algorithm was built based on the feedback compensation strategy that is theorized in this section.

Consider the motor dynamic model described by Equations 1 and 2. Equation 1 can be modified by making $T_l = 0$, and substituting $F = F(x, z, v)$,

$$J\dot{\omega}_m = K_t I - F(x, z, v) \quad (37)$$

Now suppose that the current needed to compensate for the friction force (F) is I_c . Then,

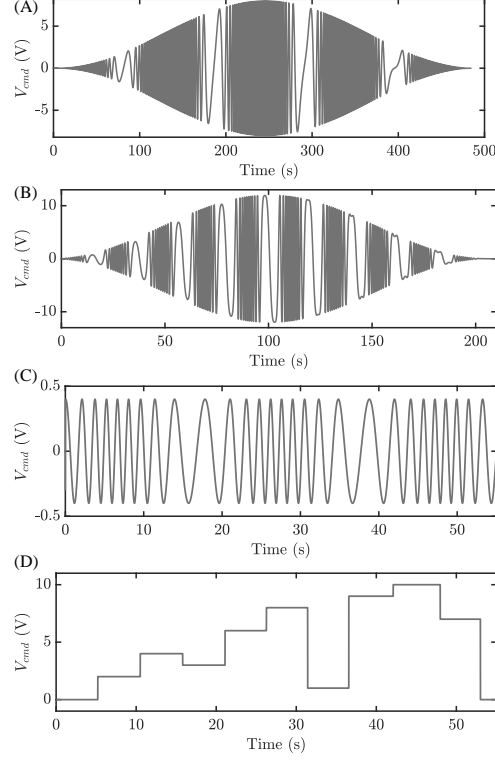


Fig. 3: The excitation signals (Commanded voltage) used for fitting and validation of motor model

$$K_t I_c = F(x, z, v) \quad (38)$$

Furthermore, if the compensation voltage necessary to generate this current is V_c , then adding this to equation 2 and modifying the new current as $I' = I + I_c$ gives,

$$L(\dot{I}') = -R(I') - K_b \omega_m + V'_{cmd} + V_c \quad (39)$$

Rearranging gives an expression for compensation voltage that must be applied to compensate for the frictional forces,

$$V_c = \dot{I}_c + R I_c \quad (40)$$

Using Equations 39 and 40, the commanded voltage can be modified so that the system behaves like a frictionless system. A block diagram representation of the friction compensation control algorithm is illustrated in Figure 4. However, if the uncertainty of the motor model parameters is high, the system could become unstable. Therefore, a stability analysis of the proposed controller was done.

6 Results

This section presents the results of the model identification and friction compensation schemes tested during the experiments on the BLDC motor described in the previous

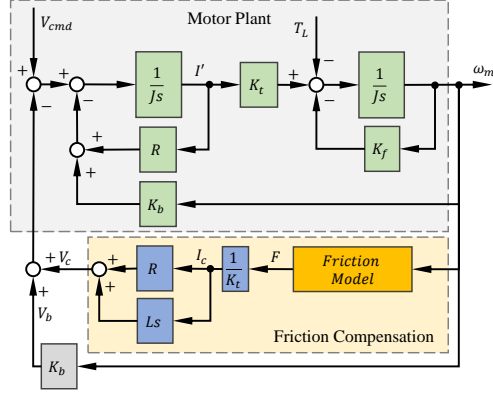


Fig. 4: Block diagram of the motor speed control algorithm with friction compensation

sections. First, the identification of LuGre model parameters using a nonlinear grey box model estimation technique is presented. It is followed by the hidden variable extraction, SINDYc model, identification results and friction compensation.

6.1 LuGre Model Identification as a Nonlinear Grey Box Model

Constant voltage signals ranging from 0.4 V to 0.6 V were given to the motor to measure the steady-state velocities. Using this data, the static parameters of the LuGre model were calculated. Later, slow voltage ramp signals with gradients ranging from 9.5 to 12 mVs^{-1} were given and the current and velocity were measured. The measured data was used to derive an initial approximation for dynamic parameters. Then nonlinear grey box model estimation technique was used to estimate more accurate values for dynamic parameters. A comparison between the measured friction value and the value predicted by the fitted model is shown in Figure 5. The estimated parameters are presented in the Table 2.

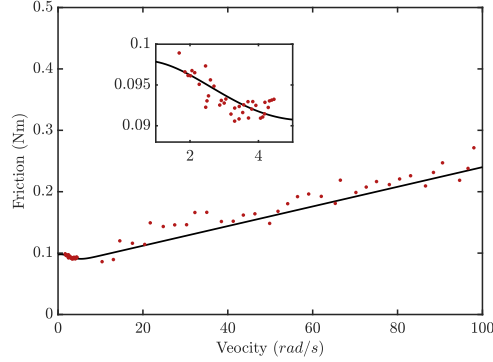


Fig. 5: Velocity vs friction data obtained from steady-state velocity experiments with fitted model

Table 2: Estimated LuGre Parameters

| α_0 | α_1 | α_2 | v_0 | σ_0 | σ_1 |
|------------|------------|------------|--------|------------|------------|
| 0.0800 | 0.0175 | 0.0016 | 3.6760 | 317.2250 | 22.2464 |

6.2 Hidden Variable Extraction from Time Delay Embedding

A high dimensional coordinate system using TDE was built using the velocity data from the excitation signal shown in Figure 3 (A). The hidden variable was then extracted using the method described in Section 5. After several trials, the order of delay embedding (m) was selected as 60, since no significant improvement could be observed for hidden variable extraction in the sense of it's resemblance to the variable values calculated using the discovered LuGre model. Figure 6 shows the singular value spectrum of the delayed coordinates, where the selected low energy range to extract the hidden variable was $k = 31$ to $k = 60$. The energy of singular values (E) is defined as the ratio between the corresponding singular value and the sum of all singular values ($\sigma_k / \sum_k \sigma_k$). The scientific reason behind this selection is the clear separation between the high energy singular values (defined as $E > 0.001$) and low energy singular values exactly at 30th value.

The rebuilt first delay coordinate from the selected low energy singular values was then compared with the z values obtained from the discovered LuGre model. The comparison is shown in Figure 7. It must be noted that the values graphed here are normalized. In the visual comparison of the values extracted from TDE and values from the LuGre model, a very good qualitative correlation can be observed, specifically, at low amplitudes (first and last 50 seconds on the graph). However, the correlation is lower at a high amplitude range (from 50 s to 150 s), for which a possible reason is the low signal-to-noise ratio (SNR) at high amplitudes. It must also be mentioned that the scale of original values obtained from TDE was scaled up by around $\times 50$ when compared with the values from LuGre model. The authors did not consider this as an issue since z variable will be incorporated with appropriate coefficients after fitting the model using SINDYc.

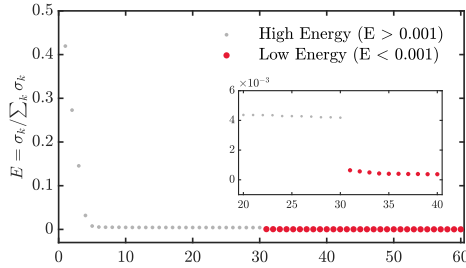


Fig. 6: Singular value spectrum obtained after k decomposing the time-delayed coordinates of the velocity data: low energy components selected to extract the hidden variable are shown in red

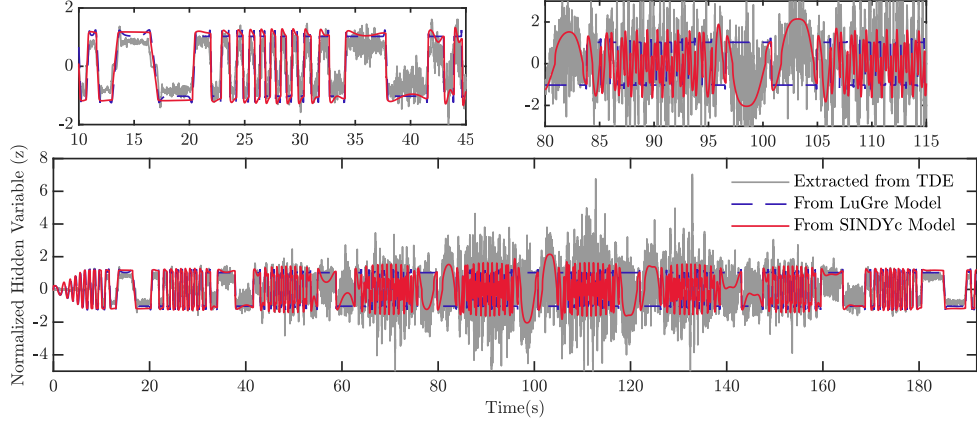


Fig. 7: Comparison of normalized hidden variable (asperity deflection) obtained using SVD of time-delayed coordinates, LuGre model and SINDYc model

6.3 SINDYc Model

The generalized SINDY algorithm for systems with control discussed in Section 5 was used to derive a nonlinear model for motor that accounts the friction.

The candidate term library $\Theta(\mathbf{X}, U)$ was composed of position (x), velocity (\dot{x}), current (I) and commanded voltage (V_{cmd}). In addition, nonlinear functions: hyperbolic tangents of velocity ($\tanh(a\dot{x})$), and hidden variable, and some other second and third-order products of velocity, hidden variable and commanded voltage were included [15]. Here a of the hyperbolic tangent function is a coefficient that ensures a close approximation of the unit step function.

$$\theta(X, U)^T = \begin{bmatrix} X \\ \dot{X} \\ Z \\ I \\ \tanh(a\dot{X}) \\ \tanh(aZ) \\ |\dot{X}|\dot{X} \\ |\dot{X}|\dot{X}^2 \\ |Z|Z \\ |Z|Z^2 \\ Z\dot{X} \\ Z^2\dot{X} \\ Z\dot{X}^2 \\ U \\ ZU \\ Z^2U \\ ZU^2 \end{bmatrix} \quad (41)$$

The sparse coefficient matrix Ξ was then obtained by the SINDYc algorithm. After iteratively omitting the small valued coefficients, it was able to make more than 1/3 of the terms sparse. The final values are shown in Equation 42.

$$\Xi = \begin{bmatrix} 0 & 0 & 0 & 0 \\ 0.87 & -16.00 & 2.49 \times 10^{-3} & -1.95 \\ -91.66 & -4331.86 & -54.39 & 118.95 \\ -1.73 & -53.76 & 0.11 & -29.87 \\ -0.49 & -8.23 & 0.55 & -0.66 \\ 0.32 & 0 & 0.14 & -0.33 \\ -3.44 \times 10^{-3} & -0.03 & -8.43 \times 10^{-5} & 7.70 \times 10^{-4} \\ 0 & -6.61 \times 10^{-6} & 0 & 0 \\ 735.63 & 50296.02 & 0 & 0 \\ 950.72 & 24866.62 & 450.07 & 997.65 \\ 0 & -12.40 & 0 & 0 \\ 0 & 188.93 & 0 & -53.11 \\ 0 & -0.18 & 0 & 8.75 \times 10^{-3} \\ 4.12 & 244.79 & 0 & 25.07 \\ 0 & 97.73 & 0 & 0 \\ 0 & 0 & 0 & 701.42 \\ 0 & -23.37 & 0 & 0 \end{bmatrix} \quad (42)$$

The four-state equations can now be written as a linear combination of the terms in the candidate term library.

$$\begin{aligned} \frac{dx}{dt} = & a_1 \dot{x} + a_2 z + a_3 I + a_4 \tanh(a\dot{x}) + a_5 \tanh(az) + a_6 |\dot{x}| \dot{x} + a_7 |z| z \\ & + a_8 |z| z^2 + a_9 u \end{aligned} \quad (43)$$

$$\begin{aligned} \frac{d\dot{x}}{dt} = & b_1 \dot{x} + b_2 z + b_3 I + b_4 \tanh(a\dot{x}) + b_5 |\dot{x}| \dot{x} + b_6 |\dot{x}| \dot{x}^2 + b_7 |z| z + b_8 |z| z^2 \\ & + b_9 z \dot{x} + b_{10} z^2 \dot{x} + b_{11} z \dot{x}^2 + b_{12} u + b_{13} zu + b_{14} zu^2 \end{aligned} \quad (44)$$

$$\frac{dz}{dt} = c_1 \dot{x} + c_2 z + c_3 I + c_4 \tanh(a\dot{x}) + c_5 \tanh(az) + c_6 |\dot{x}| \dot{x} + c_7 |z| z^2 \quad (45)$$

$$\begin{aligned} \frac{dI}{dt} = & d_1 \dot{x} + d_2 z + d_3 I + d_4 \tanh(a\dot{x}) + d_5 \tanh(az) + d_6 |\dot{x}| \dot{x} + d_7 |z| z^2 \\ & + d_8 z^2 \dot{x} + d_9 z \dot{x}^2 + d_{10} u + d_{11} z^2 u \end{aligned} \quad (46)$$

The coefficients of the Equations 43 - 46 can be found from Equation 42. One would expect Equation 43 to have only the first term i.e. the derivative of the position, but in

the fitted model it can be seen that the dynamics of position also depend on current, commanded voltage and the hidden variable. The dependency on current, voltage and a nonlinear term of velocity ($a_4 \tanh(ax) + a_6 |\dot{x}| \dot{x}$) can be interpreted as a compensation for the measurement error of velocity due to the low-resolution position sensing system used. Then the dependency on the hidden variable can be interpreted as the displacement caused by the asperity deformation that must be included in the position variable as well, but not originally included due to the low resolution of position sensors. Equation 46 suggests that velocity dynamics depend nonlinearly on velocity, hidden variable and also the commanded voltage. The dependency of commanded voltage can be interpreted as compensation for the current measurement error. Therefore the last two terms of the equation can be considered as the complementary terms for the current dependency ($b_3 I$). The remaining terms can be interpreted as components of nonlinear friction. Therefore the newly identified friction model can be written as follows,

$$F = J(b_1 \dot{x} + b_2 z + b_4 \tanh(ax) + b_5 |\dot{x}| \dot{x} + b_6 |\dot{x}| \dot{x}^2 + b_7 |z| z + b_8 |z| z^2 + b_9 z \dot{x} + b_{10} z^2 \dot{x} + b_{11} z \dot{x}^2) \quad (47)$$

The hidden variable estimated using the discovered SINDYc model has been plotted in Figure 7 together with the values obtained from the LuGre model and values extracted using TDE.

6.4 Comparison of Results

The performance of models in predicting motor states was measured using a goodness of fit function based on normalized root mean square error (NMSE) described by Equation 48 below.

$$fit = 100 \left(1 - \frac{\|y - \hat{y}\|}{\|y - \bar{y}\|} \right) \quad (48)$$

Here, y is the measured value, \hat{y} is the estimated value and \bar{y} is the mean value of y . The fit percentage values of all four models for all four excitation signals are shown in Table 3. It is noteworthy that except for the signal (C), i.e. low-velocity operation, in all other scenarios, all three models are performing at least fairly well. Out of those, the SINDYc model outperforms the other three models. For the low-velocity scenario, SINDYc outperforms all other models showing outstanding performance when compared with linear and LuGre models. To summarize, the data-driven model based on SINDYc was able to outperform the conventional linear and nonlinear models for all the cases considered.

A comparison between measured velocity and predicted velocity values from the models for the fit dataset is shown in Figure 8(A). Furthermore, the Figure 8(B) shows the responses for the first validation signal. Here, only a selected epoch of the time series data is depicted for clarity. It is observable that at low velocities, the LuGre model performs slightly better than the data-driven model, but at higher velocity values, the SINDYc-based model takes over. Thus to clarify this observation

it is important to observe the low-velocity behaviour using an excitation signal that has a low amplitude range. For this purpose, the response for the excitation signal shown in Figure 3(C) has been presented in Figure 8(C). From this graph, it is evident that LuGre model always predicts a lower value for velocity when compared with experimental values. On the other hand, the SINDYc model predicts closer and slightly lower values. Figure 8(D) shows the responses for step signal, and it can be seen that the SINDYc model outperforms the other two models.

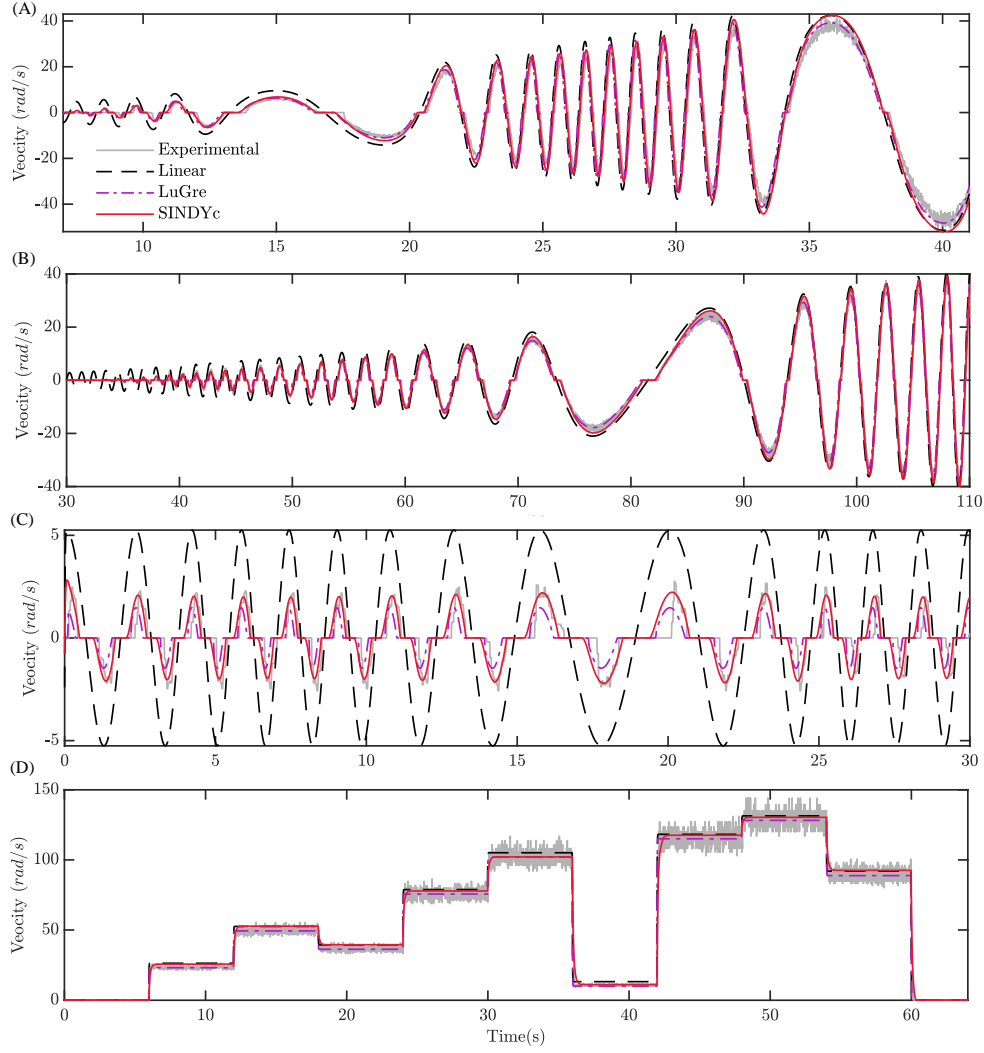
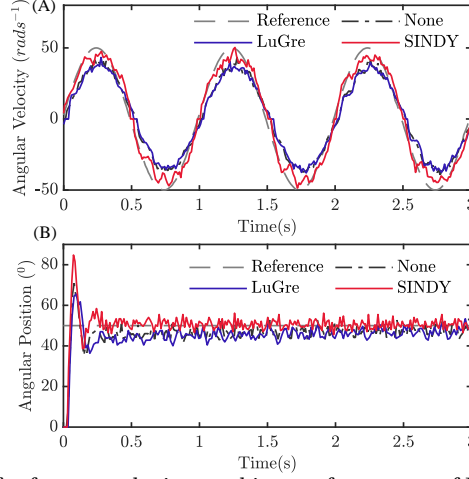


Fig. 8: Comparison of the velocity predicted by the three models: Linear, LuGre and SINDYc with the experimental data

Table 3: Fit Percentages

| Model | Model fit percentage (%) | | | | | | | |
|--------|--------------------------|-----------|-------|-----------|--------|-----------|-------|-----------|
| | (A) | | (B) | | (C) | | (D) | |
| | x | \dot{x} | x | \dot{x} | x | \dot{x} | x | \dot{x} |
| Linear | 78.43 | 73.76 | 83.89 | 75.07 | -3.713 | 16.68 | 95.78 | 86.89 |
| LuGre | 74.3 | 77.83 | 85.35 | 75.68 | -9.144 | -11.93 | 94.64 | 87.94 |
| SINDYc | 91.32 | 91.46 | 87.45 | 92.67 | 45.58 | 41.87 | 96.03 | 90.82 |

(A),(B),(C) and (D) denote the excitation signals shown in fig.3.

**Fig. 9:** Comparison of reference velocity tracking performances of LuGre and SINDYc models

6.5 Friction Compensation

The friction compensation algorithm described in Section 5 was implemented on the BLDC motor. The gain of the controller was set so that it could ensure that the system would not become unstable due to changes that happened in model parameters during the operation.

Two input cases, first a sinusoidal reference velocity signal and second a step signal were used to compare how well the velocity tracking happens in systems with and without friction compensation. The results are shown in Figure 9. The graphs also gives an insight into the superiority of the newly discovered model over the LuGre model.

7 Conclusion

This article proposes a novel nonlinear model for predicting states of an electric motor including the friction. The model was developed by applying SINDYc algorithm on position, velocity, asperity deformation and current data of a BLDC motor, which

resulted in a sparse coefficient matrix for a model with 13 nonlinear terms. Furthermore, hidden state variable of friction i.e asperity deformation, was extracted using delay embedded coordinates of motor velocity using SVD and eliminating high energy singular values.

The discovered nonlinear dynamical model was compared with the conventional linear model and a model that incorporates the LuGre friction model. The new model outperformed other two models showing superiority in predicting motor states accurately. Furthermore, the TDE based method was proven to be successful in extracting the hidden variable of friction. The developed model was then used in a feedback friction compensation algorithm to estimate friction and use that information to produce a control signal that accounts for the friction. Promising results could be obtained when compares with the LuGre model in compensating the friction.

The authors has planned to do further tests using the the discovered model based friction compensation algorithm to investigate how well it stays robust for external disturbances like varying load conditions. Further studies can be done to come up with a adaptive friction compensation algorithm that accounts for the varying load, motor orientation and temperature conditions based on the model discovery methodology formulated in this research.

References

- [1] Bona, B., Indri, M.: Friction compensation in robotics: an overview. In: Proceedings of the 44th IEEE Conference on Decision and Control, pp. 4360–4367 (2005). <https://doi.org/10.1109/CDC.2005.1582848>
- [2] Yao, J., Yang, G., Jiao, Z., Ma, D.: Adaptive robust motion control of direct-drive dc motors with continuous friction compensation. *Abstract and Applied Analysis* **2013**, 1–14 (2013) <https://doi.org/10.1155/2013/837548>
- [3] Wit, C., Olsson, H., Astrom, K.J., Lischinsky, P.: A new model for control of systems with friction. *IEEE Transactions on Automatic Control* **40**(3), 419–425 (1995) <https://doi.org/10.1109/9.376053>
- [4] Tjahjowidodo, T., Al-Bender, F., Brussel, H., Symens, W.: Friction characterization and compensation in electro-mechanical systems. *Journal of Sound and Vibration* **308**, 632–646 (2007) <https://doi.org/10.1016/j.jsv.2007.03.075>
- [5] Susanto, W., Babuška, R., Liefhebber, F., van der Weiden, T.: Adaptive friction compensation: Application to a robotic manipulator. *IFAC Proceedings Volumes* **41**(2), 2020–2024 (2008) <https://doi.org/10.3182/20080706-5-KR-1001.00343> . 17th IFAC World Congress
- [6] Al-Bender, F.: Fundamentals of friction modeling. *Proceedings - ASPE Spring Topical Meeting on Control of Precision Systems, ASPE 2010* **48** (2010)
- [7] Olsson, H., Åström, K.J., Canudas de Wit, C., Gäfvert, M., Lischinsky, P.:

- Friction models and friction compensation. *European Journal of Control* **4**(3), 176–195 (1998) [https://doi.org/10.1016/S0947-3580\(98\)70113-X](https://doi.org/10.1016/S0947-3580(98)70113-X)
- [8] Lampaert, V., Al-Bender, F., Swevers, J.: A generalized maxwell-slip friction model appropriate for control purposes. In: 2003 IEEE International Workshop on Workload Characterization (IEEE Cat. No.03EX775), vol. 4, pp. 1170–11774 (2003). <https://doi.org/10.1109/PHYCON.2003.1237071>
 - [9] Al-Bender, F., Lampaert, V., Swevers, J.: The generalized maxwell-slip model: A novel model for friction simulation and compensation. *Automatic Control, IEEE Transactions on* **50**, 1883–1887 (2005) <https://doi.org/10.1109/TAC.2005.858676>
 - [10] Nouri, B.: Friction identification in mechatronic systems. *ISA transactions* **43**, 205–16 (2004) [https://doi.org/10.1016/S0019-0578\(07\)60031-7](https://doi.org/10.1016/S0019-0578(07)60031-7)
 - [11] BALCI, M.N.: Implementation of dahl’s dynamic friction model to contact mechanics of elastic solids. *SN APPLIED SCIENCES* (2021)
 - [12] Xinli, Z., Li, X.: A finite-time robust adaptive sliding mode control for electro-optical targeting system with friction compensation. *IEEE Access* **7**, 166318–166328 (2019) <https://doi.org/10.1109/ACCESS.2019.2953997>
 - [13] Yue, F., Li, X.: Adaptive sliding mode control based on friction compensation for opto-electronic tracking system using neural network approximations. *Nonlinear Dynamics* **96**, 1–12 (2019) <https://doi.org/10.1007/s11071-019-04945-3>
 - [14] Gehb, C., Atamturktur, S., Platz, R., Melz, T.: Bayesian inference based parameter calibration of the lugre-friction model. *Experimental Techniques* **44** (2020) <https://doi.org/10.1007/s40799-019-00355-7>
 - [15] Makkar, C., Dixon, W.E., Sawyer, W.G., Hu, G.: A new continuously differentiable friction model for control systems design. In: *Proceedings, 2005 IEEE/ASME International Conference on Advanced Intelligent Mechatronics.*, pp. 600–605 (2005). <https://doi.org/10.1109/AIM.2005.1511048>
 - [16] Swevers, J., Al-Bender, F., Ganseman, C., Projogo, T.: An integrated friction model structure with improved presliding behavior for accurate friction compensation. *Automatic Control, IEEE Transactions on* **45**, 675–686 (2000) <https://doi.org/10.1109/9.847103>
 - [17] Swevers, J., Al-Bender, F., Ganseman, C.G., Projogo, T.: An integrated friction model structure with improved presliding behavior for accurate friction compensation. *IEEE Transactions on Automatic Control* **45**(4), 675–686 (2000) <https://doi.org/10.1109/9.847103>
 - [18] Iwan, W.D.: A distributed-element model for hysteresis and its steady-state dynamic response. *Journal of Applied Mechanics* **33**, 893–900 (1966)

- [19] Iskandar, M., Wolf, S.: Dynamic friction model with thermal and load dependency: modeling, compensation, and external force estimation. In: 2019 International Conference on Robotics and Automation (ICRA), pp. 7367–7373 (2019). <https://doi.org/10.1109/ICRA.2019.8794406>
- [20] Wang, S., Yu, H., Yu, J.: Robust adaptive tracking control for servo mechanisms with continuous friction compensation. *Control Engineering Practice* **87**, 76–82 (2019) <https://doi.org/10.1016/j.conengprac.2019.03.020>
- [21] Xiao, J., Zeng, F., Qiulong, Z., Liu, H.: Research on the forcefree control of cooperative robots based on dynamic parameters identification. *Industrial Robot: the international journal of robotics research and application* **ahead-of-print** (2019) <https://doi.org/10.1108/IR-01-2019-0007>
- [22] Hao, L., Pagani, R., Beschi, M., Legnani, G.: Dynamic and friction parameters of an industrial robot: Identification, comparison and repetitiveness analysis. *Robotics* **10**(1) (2021) <https://doi.org/10.3390/robotics10010049>
- [23] Ruderman, M., Krettek, J., Hoffmann, F., Bertram, T.: Optimal state space control of dc motor. (2008)
- [24] Su, Y.-R., Wang, Q., Yan, F., Huang, Y.-M.: Friction compensation for an m-level telescope based on high-precision lugre parameters identification. *Research in Astronomy and Astrophysics* **21** (2021)
- [25] Ping, Z., Zhang, W., Fu, Y.: Improved lugre-based friction modeling of the electric linear load simulator. *Journal of Physics: Conference Series* **2338**, 012079 (2022) <https://doi.org/10.1088/1742-6596/2338/1/012079>
- [26] Wang, S., Yu, H., Yu, J., Na, J., Xuemei, R.: Neural-network-based adaptive funnel control for servo mechanisms with unknown dead-zone. *IEEE Transactions on Cybernetics* **PP**, 1–12 (2018) <https://doi.org/10.1109/TCYB.2018.2875134>
- [27] Wang, Q., Zhuang, H., Duan, Z., Wang, Q.: Robust control of uncertain robotic systems: An adaptive friction compensation approach. *Science China Technological Sciences* **64**, 1228–1237 (2021)
- [28] Ramasubramanian, A., Ray, L.E.: Comparison of ekbfbased and classical friction compensation. *Journal of Dynamic Systems Measurement and Control-transactions of The Asme* **129**, 236–242 (2007)
- [29] Brisilla, R.M., Sankaranarayanan, V., A., J.G.: Extended state observer based sliding mode control of permanent magnet dc motor. In: 2015 Annual IEEE India Conference (INDICON), pp. 1–6 (2015). <https://doi.org/10.1109/INDICON.2015.7443441>
- [30] Piasek, J., Pateliski, R., Pazderski, D., Kozłowski, K.: Identification of a dynamic

- friction model and its application in a precise tracking control. *Acta Polytechnica Hungarica* **16**, 83–99 (2019) <https://doi.org/10.12700/APH.16.10.2019.10.6>
- [31] Sancak, V., Bayraktaroglu, Z.: Observer-based friction compensation in heavy-duty parallel robot control. *Journal of Mechanical Science and Technology* **35** (2021) <https://doi.org/10.1007/s12206-021-0738-2>
- [32] Brunton, S.L., Proctor, J.L., Kutz, J.N.: Discovering governing equations from data by sparse identification of nonlinear dynamical systems. *Proceedings of the National Academy of Sciences* **113**(15), 3932–3937 (2016) <https://doi.org/10.1073/pnas.1517384113> <https://www.pnas.org/doi/pdf/10.1073/pnas.1517384113>
- [33] Brunton, S., Proctor, J., Kutz, J.: Sparse identification of nonlinear dynamics with control (sindyc)**slb acknowledges support from the u.s. air force center of excellence on nature inspired flight technologies and ideas (fa9550-14-1-0398). jlp thanks bill and melinda gates for their active support of the institute of disease modeling and their sponsorship through the global good fund. jnk acknowledges support from the u.s. air force office of scientific research (fa9550-09-0174). *IFAC-PapersOnLine* **49**, 710–715 (2016) <https://doi.org/10.1016/j.ifacol.2016.10.249>
- [34] Koopman, B.O.: Hamiltonian systems and transformations in hilbert space. *Proceedings of the National Academy of Sciences of the United States of America* **17**(5), 315–318 (1931). Accessed 2023-10-27
- [35] Champion, K., Lusch, B., Kutz, J.N., Brunton, S.L.: Data-driven discovery of coordinates and governing equations. *Proceedings of the National Academy of Sciences* **116**(45), 22445–22451 (2019) <https://doi.org/10.1073/pnas.1906995116> <https://www.pnas.org/doi/pdf/10.1073/pnas.1906995116>
- [36] Hirsh, S., Ichinaga, S., Brunton, S., Kutz, J., Brunton, B.: Structured time-delay models for dynamical systems with connections to frenet–serret frame. *Proceedings of the Royal Society A: Mathematical, Physical and Engineering Sciences* **477** (2021) <https://doi.org/10.1098/rspa.2021.0097>
- [37] Brunton, S., Brunton, B., Proctor, J., Kaiser, E., Kutz, J.: Chaos as an intermittently forced linear system. *Nature Communications* **8** (2016) <https://doi.org/10.1038/s41467-017-00030-8>
- [38] Mezić, I.: Analysis of fluid flows via spectral properties of the koopman operator. *Annual Review of Fluid Mechanics* **45**, 357–378 (2013)
- [39] Bruder, D., Remy, C.D., Vasudevan, R.: Nonlinear system identification of soft robot dynamics using koopman operator theory. In: 2019 International Conference on Robotics and Automation (ICRA), pp. 6244–6250 (2019). <https://doi.org/10.1109/ICRA.2019.8793766>

- [40] Proctor, J.L., Brunton, S.L., Kutz, J.N.: Dynamic mode decomposition with control. *SIAM Journal on Applied Dynamical Systems* **15**(1), 142–161 (2016) <https://doi.org/10.1137/15M1013857> <https://doi.org/10.1137/15M1013857>
- [41] Bakarji, J., Champion, K., Kutz, J., Brunton, S.: Discovering governing equations from partial measurements with deep delay autoencoders. *Proceedings of the Royal Society A* **479** (2023) <https://doi.org/10.1098/rspa.2023.0422>
- [42] Byrd, R.H., Schnabel, R.B., Shultz, G.A.: Approximate solution of the trust region problem by minimization over two-dimensional subspaces. *Math. Program.* **40**(1-3), 247–263 (1988) <https://doi.org/10.1007/BF01580735>
- [43] Tibshirani, R.: Regression shrinkage and selection via the lasso. *Journal of the Royal Statistical Society. Series B (Methodological)* **58**(1), 267–288 (1996). Accessed 2023-10-27